Nonlocal Matrix Rank Minimization Model and Its Alternating Proximal Gradient Method for Image Inpainting

Hui-Yin Yan, and Hao Chen

***Abstract*—Image inpainting is a fundamental problem in image processing and computer vision. Due to its ill-posedness nature, regularization methods have been become a very important class of approaches for this problem. In recent years, by exploiting nonlocal low-rank prior on images, regularization methods based on low-rank minimization are widely proposed for this problem and obtained significant image restoration effects. Since the direct low-rank minimization problem suffers from solving difficulties, the matrix's rank is always replaced by its tractable approximations, such as matrix nuclear norm, weighted nuclear norm and weighted Schatten p-norm etc. In this paper, we report a novel low-rank minimization-based regularization method for the problem, in which the image inpainting model is developed by utilizing the direct matrix rank function. Although the matrix rank function makes the image inpainting model be a nonconvex and nonsmooth optimization problem. A two-blocks alternating proximal gradient algorithm is designed to solve it, and the convergence of the algorithm is proved by Kurdyka-Łojasiewicz property. Numerical results show that the proposed method can compete with some current state-of-the-art nonlocal low-rank minimization-based methods for image inpainting in terms of both image recovery quantities and visual qualities.**

***Index Terms*—image inpainting, low-rank minimization, proximal gradient method, Kurdyka-Łojasiewicz property.**

I. Introduction

Image inpainting originates from restoring of damaged old paintings or photographs with small damages such as scratches, cracks and spots, etc, [1], [2]. With the rapid evolution of computers in recent decades, it is becoming a fundamental task in image processing and computer vision domains. Since digital images are inevitably corrupted by pixels missing degradations (e. g., spots or entire blocks pixels missing) during their acquisition or transmission processes [3], [4]. Image inpainting plays an important role in many image processing and low-level vision applications, such as the restoration of old photos [5] or cultural relic images [6], preconditioning in biomedicine disciplines [7]–[9], post-production of film videos and images [10], [11], astronomical imaging [12], [13], etc.

In mathematics, the degraded image in image inpainting is modelled as

$$g = Hu + v, \tag{1}$$

where $g, u, v \in \mathbb{R}^{mn}$ are the vectors corresponding to m-by-n observed image, original clean image and zero-mean additive white Gaussian noise, respectively. $H \in \mathbb{R}^{mn\times mn}$ is a binary mask matrix related to the pixels missing degradation in g, see, [5], [6], [13]–[16].

Various methods have been proposed for image inpainting and different classifications of these methods have also been made in the literatures [1], [2]. Since it is an ill-posedness inverse problem, regularization approaches are a very important class of methods for this problem to overcome the ill-posedness nature. Regularization methods for image restoration are generally designed by exploiting different image priors, such as the local smoothness, nonlocal similarity, and sparse representation, etc, [3], [4]. Based on different image priors, it generates regularization approaches including the diffusion-based methods, exemplar-based methods, sparse representation methods, and nonlocal low-rank minimization methods. Of which, the diffusion-based algorithms are proposed by exploiting the geometrical structure information and local smooth prior on images, and complete the missing pixels by solving partial differential equations [17]–[19]. The exemplar-based methods are proposed based on image's nonlocal self-similarity prior, which assume many similar patches to a target patch existed non-locally within an image [20], [21], and the corrupted region can be restored by using information from some of its known nonlocal similar patches [5], [16], [22]. The sparse representation methods are constructed via the sparse representation prior, which posits that an image can be sparsely represented by over-redundant dictionaries and sparse coefficients. Image restoration thus involves to find suitable representation bases or sparse coefficients [23]–[25]. By combining sparse representation with nonlocal self-similarity priors, group sparse representation methods have also been proposed for image inpainting [26]. Unlike general sparse representation, group sparse representation methods adopt patch groups as the basis unit instead of single image patch to pursuit sparse representation and perform much better than many previous algorithms.

In recent years, the nonlocal low-rank prior on images has been studied and applied to image restoration. Some pioneering works can be dated back to [27], [28], where similar patches in a degraded image are matched and reshaped into column vectors to stack into a patch matching matrix. The corresponding patch matching matrix in the original clean image is believe to be low-rank and with sparse singular values. As a consequence, image restoration is transformed into a matrix rank minimization

Manuscript received June 4, 2025; revised July 28, 2025.

This work was supported in part by Nanhu Scholar Program for Young Scholars of XYNU.

Hui-Yin Yan is a lecturer at the School of Mathematics and Statistics, Xinyang Normal University, Xinyang, 464000, P. R. China (Corresponding author, E-mail: yanhuiyin@xynu.edu.cn).

Hao Chen is a postgraduate at the School of Mathematics and Statistics, Xinyang Normal University, Xinyang, 464000, P. R. China (E-mail: 534361090@qq.com).

problem [29], [30]. Since the direct rank minimization problem is a NP hard problem and surfers from significant computational challenges. Numerous surrogates have been proposed to approximate the matrix rank in the problem and provide feasible solutions. For example, the nuclear norm, defined as the sum of all singular values of a matrix, has been proven to be the tightest convex relaxation of the matrix's rank [30]. By utilizing the F-norm date term nuclear norm minimization (NNM, nuclear norm minimization) model [29], Ji et al. [27] developed a NNM-based method for video image denoising. Although NNM model provides a convex approximation, and it also results a closed-form solution which can be solved via a singular value decomposition (SVD, singular value decomposition)-based soft-thresholding algorithm [29]. However, there are biases in the optimal rank minimization estimation. Because the largest singular values constitute the most important part of a matrix's rank, and the SVD-based soft-thresholding algorithm shrinks them equally. To overcome this drawback, the weighted nuclear norm minimization (WNNM, weighted nuclear norm minimization) model was further proposed by introducing different weights to different singular values in nuclear norm. WNNM model can be solved by an SVD-based weighted soft-thresholding algorithm, which is able to treat different singular values differently [31]. Owing to this advantage, WNNM model has been demonstrated impressive restoration effects in tasks such as image denoising, deblurring, and inpainting [31]–[36]. Besides, similar to matrix nuclear norm and weighted nuclear norm, the matrix Schatten p-norm was proposed in [37], which is in fact the vector Schatten p-norm defined on singular values of a matrix. In [38], matrix Schatten p-norm minimization model [37] was extended to a weighted Schatten p-norm minimization (WSNM, weighted Schatten p-norm minimization) model and further applied to image denoising and background subtraction problems. In [39], a truncated nuclear norm minimization (TNNM, truncated nuclear norm minimization) model was proposed and the truncated nuclear norm is defined to be the sum of few largest singular values of a matrix. By using TNNM to characterize nonlocal low-rank prior on images, a nonconvex TNNM-based regularization model was developed and solved by using an efficient alternating direction method of multipliers in [40]. In addition, the relationships between patch-based group sparse representation and nonlocal low-rank prior were discussed in the literatures [41], [42] and the WSNM was adopted to develop the final image restoration models and algorithms.

In this paper, we propose a novel nonlocal low-rank minimization method for image inpainting. This work is inspired by our previous works in [43], where an F-norm data term matrix rank minimization (RM, rank minimization) model was proposed and solved by a SVD-based hard-thresholding algorithm. By leveraging the advantages of image nonlocal self-similarity, the RM model have been successfully applied to image denoising problems, such as Gaussian white additive noise removal and multiplicative Gamma noise removal problems, and significant image denoising results have been achieved. Here, we further extend the application of the RM model for image inpainting, and construct a regularization method for this problem. The method mainly includes a RM-based regularization model and its alternating proximal gradient solving algorithm. The energy function of the RM-based regularization model consists the sum of all patch matching matrices' rank and a L_2 norm date fidelity term. Although the matrix rank terms render the image restoration model a nonconvex and nonsmooth optimization problem. An alternating proximal gradient algorithm is designed to solve it. With the matrix rank function satisfying the famous Kurdyka-Łojasiewicz property, the global convergence of the alternating proximal gradient algorithm can be well analyzed and proved. Numerical results show that the proposed method can outperform some current state-of-the-art nonlocal low-rank methods for image inpainting.

Compared to WNNM, TNNM, and WSNM-based methods, we highlight two advantages of using direct matrix's rank to construct a nonlocal low-rank minimization method for image inpainting. First, it successfully avoids the tedious weight parameters in the WNNM, TNNM, and WSNM-based image restoration models, and also can achieve a more accurate low-rank estimation than them. Second, the reduced weight parameters makes the solving of the RM-based image restoration model much easier than that of WNNM, TNNM, and WSNM-based image restoration models, and also facilitates the analysis of the global convergence of the iterative solving algorithm. The main contributions of this paper are as follows.

- A novel nonlocal low-rank minimization model is developed for image inpainting using direct matrix rank minimization.
- An alternating proximal gradient algorithm is designed to solve the proposed nonconvex and nonsmooth RM-based image restoration model.
- The convergence of the alternating proximal gradient algorithm is analyzed and proved based on the famous Kurdyka-Łojasiewicz property.
- Numerical results demonstrate that the proposed method can perform better than some current state-of-the-art nonlocal low-rank minimization methods for image inpainting.

The rest of the paper is organized as follows. In Section 2, a novel nonlocal RM-based image inpainting model is constructed. In Section 3, an alternating proximal gradient algorithm is developed to solve the nonlocal RM-based image inpainting model. The convergence of the proposed alternating proximal gradient algorithm is analyzed and proved in Section 4. Numerical experiments are shown in Section 5 to demonstrate the effectiveness of the proposed image inpainting method. Finally, concluding remarks are given in Section 6.

II. RM-based Regularization Model for Image Inpainting

In this section, we propose a RM-based regularization model for image inpainting. Based on image nonlocal similarity, for a local $\sqrt{s}$-by-$\sqrt{s}$ patch g_i in g, we can extract its $t-1$ most similar patches $g_i^2, \cdots, g_i^t$ in the image. By reshaping these image patches into column

vectors, a s-by-t patch matching matrix can be formed as

$$M_i = [\mathcal{V}g_i, \mathcal{V}g_i^2, \cdots, \mathcal{V}g_i^t],$$

where $\mathcal{V}$ is denoted as the operator that reshapes the corresponding matrix column by column into a vector. Since each element of M_i is extracted from the degraded image g, there must exist a binary matrix $R_i \in \mathbb{R}^{st\times mn}$ with elements being 0 or 1, such that

$$\mathcal{V}M_i = R_i g \in \mathbb{R}^{st},$$

where $\mathcal{V}M_i$ is the stacked vector by columns of M_i. The binary matrix R_i is called as the matching patch extracting matrix to the reference patch g_i. By introducing another reshaping operator $\mathcal{M}$, which reshapes a matrix column by column into a vector. It satisfies that

$$\mathcal{M}R_i g = M_i,$$

and thus $\mathcal{M}R_i u$ are the low-rank matrix in the clean image u corresponding to M_i.

Suppose there have p reference patches g_i $(i = 1, 2, \cdots, p)$ in g. By minimizing the sum of the rank of each $\mathcal{M}R_i u$, we construct the RM-based regularization model for image inpainting as

$$\min_u \ \frac{1}{2}\|Hu - g\|_2^2 + \sum_{i=1}^{p}\omega_i \mathrm{rank}(\mathcal{M}R_i u), \tag{2}$$

where $\|Hu - g\|_2^2$ is the generally used L_2-norm date fidelity term, $\sum_{i=1}^{p}\omega_i \mathrm{rank}(\mathcal{M}R_i u)$ is the RM-based regularization term, ω_i $(i = 1, 2, \cdots, p)$ are the corresponding regularization related parameters.

For the sake of efficient methods to solve model (2), we introduce the auxiliary variable matrices $X_i \in \mathbb{R}^{s\times t}$ to patch matching matrixes $\mathcal{M}R_i u$ for $i = 1, 2, \cdots, p$. By using the variable splitting and half quadratic penalty techniques, (2) can be solved by the following optimization problem

$$\min_{(X,u)} \ \mathcal{J}(X, u), \tag{3}$$

and

$$\begin{aligned}\mathcal{J}(X, u) = \ & \frac{1}{2}\|Hu - g\|_2^2 \\ & + \frac{\lambda}{2}\sum_{i=1}^{p}\|X_i - \mathcal{M}R_i u\|_F^2 + \sum_{i=1}^{p}\omega_i \mathrm{rank}(X_i),\end{aligned}$$

where $X = (X_1, X_2, \cdots, X_p)$ and λ is a positive constant. Based on the ideals of half quadratic penalty method, as $\lambda \to \infty$, the solution of (3) approaches that of (2).

III. Alternating Proximal Gradient Method

Denote by

$$\mathcal{Q}(u) = \frac{1}{2}\|Hu - g\|_2^2, \quad \mathcal{H}(X, u) = \sum_{i=1}^{p}\mathcal{H}_i(X, u),$$

and

$$\mathcal{H}_i(X, u) = \frac{\lambda}{2}\|X_i - \mathcal{M}R_i u\|_F^2, \quad i = 1, 2, \cdots, p.$$

The objection function $\mathcal{J}$ in (3) can be reformulated as

$$\mathcal{J}(X, u) = \mathcal{Q}(u) + \mathcal{H}(X, u) + \sum_{i=1}^{p}\omega_i \mathrm{rank}(X_i).$$

Since $X_1, X_2, \cdots, X_p$ and $\mathcal{H}_1(X, u)$, $\mathcal{H}_2(X, u)$, $\cdots$, $\mathcal{H}_p(X, u)$ in $\mathcal{H}$ and $\mathcal{J}$ are separable. Each $\mathcal{H}_i(X, u)$ has the second order differentiable about variables X_i and $R_i u$. Next, we introduce an alternating proximal gradient minimization scheme to solve (3).

Starting from an initial guess $\left(X^{(0)}, u^{(0)}\right)$ with $X^{(0)} = \left(X_1^{(0)}, X_2^{(0)}, \cdots, X_p^{(0)}\right)$, the k-th iteration of the method is to solve $X^{(k)} = \left(X_1^{(k)}, X_2^{(k)}, \cdots, X_p^{(k)}\right)$ and $u^{(k)}$,

$$\begin{cases} X_1^{(k)} \in \arg\min\limits_{X_1} \dfrac{\alpha_1}{2}\left\|X_1 - X_1^{(k-1)}\right\|_F^2 + \omega_1 \mathrm{rank}(X_1) \\ \qquad + \left\langle \nabla_{X_1}\mathcal{H}\left(X^{(k-1)}, u^{(k-1)}\right), X_1 - X_1^{(k-1)}\right\rangle; \\ X_2^{(k)} \in \arg\min\limits_{X_2} \dfrac{\alpha_2}{2}\left\|X_2 - X_2^{(k-1)}\right\|_F^2 + \omega_2 \mathrm{rank}(X_2) \\ \qquad + \left\langle \nabla_{X_2}\mathcal{H}\left(X^{(k-1)}, u^{(k-1)}\right), X_2 - X_2^{(k-1)}\right\rangle; \\ \qquad \vdots \\ X_p^{(k)} \in \arg\min\limits_{X_p} \dfrac{\alpha_p}{2}\left\|X_p - X_p^{(k-1)}\right\|_F^2 + \omega_p \mathrm{rank}(X_p) \\ \qquad + \left\langle \nabla_{X_p}\mathcal{H}\left(X^{(k-1)}, u^{(k-1)}\right), X_p - X_p^{(k-1)}\right\rangle; \\ u^{(k)} = \arg\min\limits_{u} \mathcal{Q}(u) + \dfrac{\beta}{2}\sum\limits_{i=1}^{p}\left\|R_i u - R_i u^{(k-1)}\right\|_2^2 \\ \qquad + \sum\limits_{i=1}^{p}\left\langle \nabla_{R_i u}\mathcal{H}\left(X^{(k)}, u^{(k-1)}\right), R_i u - R_i u^{(k-1)}\right\rangle; \end{cases} \tag{4}$$

where $\langle\cdot\rangle$ is the inner product of the vectors or matrices, ∇ is the gradient operator of the corresponding function. $\alpha_1, \alpha_2, \cdots, \alpha_p, \beta$ are the positive relaxation parameters in the algorithm, which are generally selected larger than the lipschitz constants of $\mathcal{H}$ with respective to variables $X_1, X_2, \cdots, X_p$ and u. By a complete squared derivation, (4) can be reformulated as

$$\begin{cases} X_1^{(k)} \in \arg\min\limits_{X_1} \omega_1 \mathrm{rank}(X_1) \\ \qquad + \dfrac{\alpha_1}{2}\left\|X_1 - \dfrac{\varrho_1}{\alpha_1}X_1^{(k-1)} - \dfrac{\lambda}{\alpha_1}\mathcal{M}R_1 u^{(k-1)}\right\|_F^2; \\ X_2^{(k)} \in \arg\min\limits_{X_2} \omega_2 \mathrm{rank}(X_2) \\ \qquad + \dfrac{\alpha_2}{2}\left\|X_2 - \dfrac{\varrho_2}{\alpha_2}X_2^{(k-1)} - \dfrac{\lambda}{\alpha_2}\mathcal{M}R_2 u^{(k-1)}\right\|_F^2; \\ \qquad \vdots \\ X_p^{(k)} \in \arg\min\limits_{X_p} \omega_p \mathrm{rank}(X_p) \\ \qquad + \dfrac{\alpha_p}{2}\left\|X_p - \dfrac{\varrho_p}{\alpha_p}X_p^{(k-1)} - \dfrac{\lambda}{\alpha_p}\mathcal{M}R_p u^{(k-1)}\right\|_F^2; \\ u^{(k)} = \arg\min\limits_{u} \dfrac{1}{2}\|Hu - g\|_2^2 \\ \qquad + \sum\limits_{i=1}^{p}\dfrac{\beta}{2}\left\|R_i u - \dfrac{\varrho}{\beta}R_i u^{(k-1)} - \dfrac{\lambda}{\beta}\mathcal{V}X_i^{(k)}\right\|_2^2; \end{cases} \tag{5}$$

where $\varrho_i = \alpha_i - \lambda, i = 1, 2, \cdots, p$ and $\varrho = \beta - \lambda$. For $i = 1, 2, \cdots, p$, suppose it has the SVD decomposition

$$\frac{\varrho_i}{\alpha_i}X_i^{(k-1)} + \frac{\lambda}{\alpha_i}\mathcal{M}R_i u^{(k-1)} = U_i^{(k-1)}\Sigma_i^{(k-1)}\left(V_i^{(k-1)}\right)^T.$$

Taking advantages of the SVD-based hard-thresholding algorithm in [43], each $X_i^{(k)}$ in (5) can be solved as

$$X_i^{(k)} = U_i^{(k-1)} \mathcal{D}_{\frac{\omega_i}{\alpha_i}} \left(\Sigma_i^{(k-1)} \right) \left(V_i^{(k-1)} \right)^T, \ i = 1, 2, \cdots, p.$$

Where $\mathcal{D}_\tau(\Sigma)$ is the hard thresholding function defined on a diagonal matrix Σ with parameter τ, and for each diagonal element Σ_{ii} in Σ,

$$\mathcal{D}_\tau(\Sigma)_{ii} = \begin{cases} \Sigma_{ii}, & \text{for } \Sigma_{ii} \geq \sqrt{2\tau}, \\ 0, & \text{for } \Sigma_{ii} < \sqrt{2\tau}, \end{cases}$$

see, for instance [43].

Since $u^{(k)}$ in (5) is the minimizer point of a quadratic function. Based on the first order differential condition, it can be solved by linear system

$$(H^T H + \beta W)u = H^T g + \varrho W u^{(k-1)} + \lambda \sum_{i=1}^{p} R_i^T \mathcal{V} X_i^{(k)},$$

where $W = \sum_{i=1}^{p} R_i^T R_i$, and $W \in \mathbb{R}^{mn \times mn}$ is a diagonal matrix with each diagonal entry being the extracting times of corresponding pixel in the image. Due to the reference patches overlapped the whole image, the diagonal values of W must be integers no less than one. As a consequence,

$$u^{(k)} = A^{-1} \left(H^T g + \varrho W u^{(k-1)} + \lambda \sum_{i=1}^{p} R_i^T \mathcal{V} X_i^{(k)} \right),$$

where $A = H^T H + \beta W$ is a positive definite symmetric matrix.

IV. Convergence Analysis

In this section, we show the convergence of the proposed alternating proximal gradient method (5). Our convergence analysis is based on the famous Kurdyka-Łojasiewicz property. Denote $\|\cdot\|$ as the Euclidean norm, we refer the definitions of Fréchet subdifferential [44] and Kurdyka-Łojasiewicz property firstly.

The Fréchet subdifferential is in fact consistent with the classical differential for continuously differentiable function. Specifically, the well-known Fermat's rule with respective to continuously differentiable functions is unchanged under the definition of Fréchet subdifferential. Without loss of generality, the subdifferential of function f at a point x is denoted by $\partial f(x)$. Thus, the necessary but not sufficient condition for $x \in \mathbb{R}^d$ to be a local minimizer of f is $\mathbf{0} \in \partial f(x)$, where $\mathbf{0}$ is the corresponding zero point.

The Kurdyka-Łojasiewicz property was originally proposed by Łojasiewicz and Kurdyka, and further developed by Bolte et al., which has wide applications in nonconvex and nonsmooth optimization problems [45]–[48]. Checking whether a function has the Kurdyka-Łojasiewicz property at some given point is, in fact, a challenge task. However, the Kurdyka-Łojasiewicz functions which have the Kurdyka-Łojasiewicz property at each point of their domains are ubiquitous, such as uniformly convex functions, convex functions with growth conditions, metric regularities, constraint qualifications, and semialgebraic and definable functions, see, [45]–[49].

Since it has been proved that the matrix rank function is a semi-algebraic function [50], and semi-algebraic functions under operations of finite sums, products, scalar products and compositions are still semi-algebraic function [46], [47], [49]. The objective function $\mathcal{J}$ in (3) is clearly a semi-algebraic and Kurdyka-Łojasiewicz function.

Next, we develop the convergence theory of the proposed alternating proximal gradient algorithm by the Kurdyka-Łojasiewicz property of $\mathcal{J}$.

Theorem 1: Suppose $\left\{\xi^{(k)}\right\}$ is a sequence generated by the proposed alternating minimization method (5), with $\xi^{(k)} = \left(X^{(k)}, u^{(k)}\right)$ and $X^{(k)} = \left(X_1^{(k)}, X_2^{(k)}, \cdots, X_p^{(k)}\right)$. For $k \geq 1$, it satisfies

$$\mathcal{J}\left(\xi^{(k)}\right) + \sum_{i=1}^{p} \frac{\varrho_i}{2} \left\| X_i^{(k)} - X_i^{(k-1)} \right\|_F^2 + \frac{\varrho}{2} \sum_{i=1}^{p} \left\| R_i u^{(k)} - R_i u^{(k-1)} \right\|_2^2 \leq \mathcal{J}\left(\xi^{(k-1)}\right), \quad (6)$$

namely, $\mathcal{J}\left(\xi^{(k)}\right)$ dose not increase, and more over

$$\lim_{k \to \infty} \left\| \xi^{(k)} - \xi^{(k-1)} \right\|^2 = 0. \quad (7)$$

Proof: Since each $\mathcal{H}_i(X, u)$ has second order differentiable about variables X_i and $R_i u$. We have the Taylor expansions

$$\mathcal{H}_i\left(X, u^{(k-1)}\right) = \mathcal{H}_i\left(X, u^{(k-1)}\right) + \frac{\lambda}{2} \left\| X_i - X_i^{(k-1)} \right\|_F^2 + \left\langle \nabla_{X_i} \mathcal{H}_i\left(X^{(k-1)}, u^{(k-1)}\right), X_i - X_i^{(k-1)} \right\rangle, \quad (8)$$

and

$$\mathcal{H}_i\left(X^{(k)}, u\right) = \mathcal{H}_i\left(X^{(k)}, u^{(k-1)}\right) + \left\langle \nabla_{R_i u} \mathcal{H}_i\left(X^{(k)}, u^{(k-1)}\right), R_i u - R_i u^{(k-1)} \right\rangle + \frac{\lambda}{2} \left\| R_i u - R_i u^{(k-1)} \right\|_2^2, \quad (9)$$

for $i = 1, 2, \cdots, p$. Combined (8), (9) with (4), it can be derived that

$$X_i^{(k)} \in \arg\min_{X_i} \ \mathcal{H}_i\left(X, u^{(k-1)}\right) + \omega_i \mathrm{rank}(X_i) + \frac{\varrho_i}{2} \left\| X_i - X_i^{(k-1)} \right\|_F^2, \quad i = 1, 2, \cdots, p, \quad (10)$$

and

$$u^{(k)} = \arg\min_{u} \ Q(u) + \sum_{i=1}^{p} \mathcal{H}_i\left(X^{(k)}, u^{(k-1)}\right) + \frac{\varrho}{2} \sum_{i=1}^{p} \left\| R_i u - R_i u^{(k-1)} \right\|_2^2. \quad (11)$$

Therefore,

$$X^{(k)} \in \arg\min_{X} \ \mathcal{J}\left(X, u^{(k-1)}\right) + \sum_{i=1}^{p} \frac{\varrho_i}{2} \left\| X_i - X_i^{(k-1)} \right\|_F^2, \quad (12)$$

and

$$u^{(k)} \in \arg\min_{X} \ \mathcal{J}\left(X^{(k)}, u\right) + \frac{\varrho}{2} \sum_{i=1}^{p} \left\| R_i u - R_i u^{(k-1)} \right\|_2^2. \quad (13)$$

As a consequence of (12) and (13),

$$\mathcal{J}\left(X^{(k)},u^{(k-1)}\right)+\sum_{i=1}^{p}\frac{\varrho_i}{2}\left\|X_i^{(k)}-X_i^{(k-1)}\right\|_F^2 \leq \mathcal{J}\left(X^{(k-1)},u^{(k-1)}\right),$$

and

$$\mathcal{J}\left(X^{(k)},u^{(k)}\right)+\frac{\varrho}{2}\sum_{i=1}^{p}\left\|R_iu-R_iu^{(k-1)}\right\|_2^2 \leq \mathcal{J}\left(X^{(k)},u^{(k-1)}\right).$$

Adding above two inequalities, it satisfies

$$\mathcal{J}\left(X^{(k)},u^{(k)}\right)+\sum_{i=1}^{p}\frac{\varrho_i}{2}\left\|X_i^{(k)}-X_i^{(k-1)}\right\|_F^2 + \frac{\varrho}{2}\sum_{i=1}^{p}\left\|R_iu-R_iu^{(k-1)}\right\|_2^2 \leq \mathcal{J}\left(X^{(k-1)},u^{(k-1)}\right). \tag{14}$$

By adding inequality (14) from $k=1$ to some $k=K$,

$$\sum_{k=1}^{K}\left(\sum_{i=1}^{p}\frac{\varrho_i}{2}\left\|X_i^{(k)}-X_i^{(k-1)}\right\|_F^2 +\frac{\varrho}{2}\sum_{i=1}^{p}\left\|R_iu-R_iu^{(k-1)}\right\|_2^2\right) \leq \mathcal{J}\left(\xi^{(0)}\right)-\mathcal{J}\left(\xi^{(K)}\right).$$

Since $\varrho_1,\varrho_2,\cdots,\varrho_p,\varrho$ are bounded positive constants, and

$$\left\|u-u^{(k-1)}\right\|_2^2 < \sum_{i=1}^{p}\left\|R_iu-R_iu^{(k-1)}\right\|_2^2,$$

(7) is definitely satisfied. ■

Theorem 2: Suppose $\left\{\xi^{(k)}\right\}$ is a sequence generated by the proposed alternating minimization method (5), with $\xi^{(k)}=\left(X^{(k)},u^{(k)}\right)$ and $X^{(k)}=\left(X_1^{(k)},X_2^{(k)},\cdots,X_p^{(k)}\right)$. For $k\geq 1$, denote by

$$\widehat{X_i}^{(k)}=-\alpha_i\left(X_i^{(k)}-X_i^{(k-1)}\right)-\lambda\mathcal{M}R_i\left(u^{(k)}-u^{(k-1)}\right),$$

for $i=1,2,\cdots,p$, and

$$\widehat{u}^{(k)}=-\varrho W\left(u^{(k)}-u^{(k-1)}\right).$$

Then, it holds that

$$\widehat{\xi}^{(k)}=\left(\widehat{X_1}^{(k)},\widehat{X_2}^{(k)},\cdots\widehat{X_p}^{(k)},\widehat{u}^{(k)}\right)\in\partial\mathcal{J}\left(\xi^{(k)}\right),$$

and

$$\left\|\widehat{\xi}^{(k)}\right\|\leq c\left\|\xi^{(k)}-\xi^{(k-1)}\right\|, \tag{15}$$

where c is a bounded positive constant.

Proof: Since $X_1^{(k)},X_2^{(k)},\cdots,X_p^{(k)}$ and $u^{(k)}$ are minimizers of (10) and (11). For $k\geq 1$, (10) suggests that

$$\mathbf{0}\in\lambda\left(X_i^{(k-1)}-\mathcal{M}R_iu^{(k-1)}\right)+\varrho_i\left(X_i^{(k)}-X_i^{(k-1)}\right)+\omega_i\partial\mathrm{rank}\left(X_i^{(k)}\right),\quad i=1,2,\cdots,p. \tag{16}$$

where $\mathbf{0}\in\mathbb{R}^{s\times t}$ and $\partial\mathrm{rank}\,(\cdot)$ is the subdifferential of the corresponding matrix rank function. Then, by adding $-\lambda\mathcal{M}R_i\left(u^{(k)}-u^{(k-1)}\right)+\lambda\left(X_i^{(k)}-X_i^{(k-1)}\right)$ in both sides of formulation (16), we can derive that

$$-\alpha_i\left(X_i^{(k)}-X_i^{(k-1)}\right)-\lambda\mathcal{M}R_i\left(u^{(k)}-u^{(k-1)}\right)\in\lambda\left(X_i^{(k)}-\mathcal{M}R_iu^{(k)}\right)+\omega\partial\mathrm{rank}\left(X_i^{(k)}\right), \tag{17}$$

for $i=1,2,\cdots,p$. Therefore, for $k\geq 1$,

$$\begin{aligned}\widehat{X_i}^{(k)} &\in \lambda\left(X_i^{(k)}-\mathcal{M}R_iu^{(k)}\right)+\omega\partial\mathrm{rank}\left(X_i^{(k)}\right)\\ &= \partial_{X_i}\mathcal{J}\left(X^{(k)},u^{(k)}\right),\quad i=1,2,\cdots,p.\end{aligned} \tag{18}$$

Analogously, for all $k\geq 1$, (11) suggests that

$$\mathbf{0}=\nabla_u\mathcal{Q}(u^{(k)})-\lambda\sum_{i=1}^{p}R_i^T\left(\mathcal{V}X_i^{(k)}-R_iu^{(k)}\right)+\varrho W\left(u^{(k)}-u^{(k-1)}\right),$$

and

$$\begin{aligned}\widehat{u}^{(k)} &= \nabla_u\mathcal{Q}(u^{(k)})-\lambda\sum_{i=1}^{p}R_i^T\left(\mathcal{V}X_i^{(k)}-R_iu^{(k)}\right)\\ &= \nabla_u\mathcal{J}\left(X^{(k)},u^{(k)}\right).\end{aligned} \tag{19}$$

For some $\xi=(X_1,X_2,\cdots,X_p,u)\in\mathrm{dom}\mathcal{J}$, the subdifferential calculation formulations of variable separated functions [44] suggests that,

$$\partial\mathcal{J}(\xi)=\partial_{X_1}\mathcal{J}(\xi)\times\partial_{X_2}\mathcal{J}(\xi)\times\cdots\times\partial_{X_p}\mathcal{J}(\xi)\times\partial_u\mathcal{J}(\xi).$$

Hence, (18) and (19) imply that

$$\widehat{\xi}^{(k)}=\left(\widehat{X}_1^{(k)},\widehat{X}_2^{(k)},\cdots\widehat{X}_p^{(k)},\widehat{u}^{(k)}\right)\in\partial\mathcal{J}\left(\xi^{(k)}\right).$$

Moreover, for all $k\geq 1$, it can be further derived that

$$\begin{aligned}\left\|\widehat{\xi}^{(k)}\right\| &\leq \lambda\sum_{i=1}^{p}\left\|\mathcal{M}R_i\left(u^{(k)}-u^{(k-1)}\right)\right\|_F\\ &+\sum_{i=1}^{p}\alpha_i\left\|X_i^{(k)}-X_i^{(k-1)}\right\|_F+\varrho\left\|W\left(u^{(k)}-u^{(k-1)}\right)\right\|_2\\ &\leq \left(\alpha_{\max}+\lambda\rho\left(W^{\frac{1}{2}}\right)+\varrho\rho(W)\right)\left\|\xi^{(k)}-\xi^{(k-1)}\right\|,\end{aligned}$$

where $\alpha_{\max}$ is the maximum value of $\alpha_1,\alpha_2,\cdots,\alpha_p$, and $\rho(\cdot)$ is the spectral norm of the matrix. ■

Theorem 3: Suppose $\left\{\xi^{(k)}\right\}$ is a sequence generated by the proposed alternating minimization method (5), with $\xi^{(k)}=\left(X^{(k)},u^{(k)}\right)$ and $X^{(k)}=\left(X_1^{(k)},X_2^{(k)},\cdots,X_p^{(k)}\right)$, $\mathcal{S}$ is the limit point set of $\left\{\xi^{(k)}\right\}$. If $\left\{\xi^{(k)}\right\}$ is a bounded sequence, then,

(i) $\mathcal{S}$ is a nonempty compact and connected set,

$$\lim_{k\to+\infty}\mathrm{dist}\left(\xi^{(k)},\mathcal{S}\right)\to 0;$$

(ii) $\mathcal{S}\subset\mathrm{crit}\mathcal{J}$;

(iii) $\mathcal{J}$ is finite and constant on $\mathcal{S}$, and which equals to

$$\inf_{k\in N}\mathcal{J}(\xi^{(k)})=\lim_{k\to\infty}\mathcal{J}(\xi^{(k)}).$$

Proof: Based on (7) and the classical properties of bounded sequences, the conclusion (i) is certainly satisfied.

For any $X=(X_1,X_2,\cdots,X_p)$ and $u\in\mathbb{R}^{mn}$, it can be

derived by (12) and (13) that

$$\mathcal{J}\left(X^{(k)},u^{(k-1)}\right)+\sum_{i=1}^{p}\frac{\varrho_i}{2}\left\|X_i^{(k)}-X_i^{(k-1)}\right\|_F^2 \leq \mathcal{J}\left(X,u^{(k-1)}\right)+\sum_{i=1}^{p}\frac{\varrho_i}{2}\left\|X_i-X_i^{(k-1)}\right\|_F^2,$$

and

$$\mathcal{J}\left(X^{(k)},u^{(k)}\right)+\frac{\varrho}{2}\sum_{i=1}^{p}\left\|R_iu^{(k)}-R_iu^{(k-1)}\right\|_2^2 \leq \mathcal{J}\left(X^{(k)},u\right)+\frac{\varrho}{2}\sum_{i=1}^{p}\left\|R_iu-R_iu^{(k-1)}\right\|_2^2.$$

Adding above two inequalities and setting $u=u^{(k-1)}$, it can obtain that

$$\mathcal{J}\left(X^{(k)},u^{(k)}\right)+\frac{\varrho_{\min}}{2}\left\|\xi^{(k)}-\xi^{(k-1)}\right\|^2 \leq \mathcal{J}\left(X,u^{(k-1)}\right)+\sum_{i=1}^{p}\frac{\varrho_i}{2}\left\|X_i-X_i^{(k-1)}\right\|_F^2, \quad (20)$$

where $\varrho_{\min}$ is the minimum value of ϱ_i $(i=1,2,\cdots,p)$ and ϱ. Suppose $\xi^*=\left(X_1^*,X_2^*,\cdots,X_p^*,u^*\right)$ to be some point in $\mathcal{S}$, then there must exist a subsequence $\left\{\xi^{(k')}\right\}$ of $\left\{\xi^{(k)}\right\}$ and which converges to ξ^*. Considering of $k=k'$ and $X=\left(X_1^*,X_2^*,\cdots,X_p^*\right)$ in (20), we have

$$\mathcal{J}\left(X^{(k')},u^{(k')}\right)+\frac{\varrho_{\min}}{2}\left\|\xi^{(k')}-\xi^{((k-1)')}\right\|^2 \leq \mathcal{J}\left(X^*,u^{((k-1)')}\right)+\sum_{i=1}^{p}\frac{\varrho_i}{2}\left\|X_i^*-X_i^{((k-1)')}\right\|_F^2. \quad (21)$$

Cause $\mathcal{J}$ is continuous about u, by (7) and (21),

$$\lim\mathcal{J}\left(X^{(k')},u^{(k')}\right)\leq\mathcal{J}\left(X^*,u^*\right).$$

However, $\mathcal{J}$ is a lower semicontinuous function,

$$\lim\mathcal{J}\left(X^{(k')},u^{(k')}\right)\geq\mathcal{J}\left(X^*,u^*\right).$$

Therefore, it holds

$$\lim\mathcal{J}\left(X^{(k')},u^{(k')}\right)=\mathcal{J}\left(X^*,u^*\right).$$

Denote by

$$\widehat{\xi}^{(k')}=\left(\widehat{X_1}^{(k')},\widehat{X_2}^{(k')},\cdots\widehat{X_p}^{(k')},\widehat{u}^{(k')}\right),$$

and which is the same definition as that in Theorem 1. Then, by (15), $\widehat{\xi}^{(k')}\in\partial\mathcal{J}\left(\xi^{(k')}\right)$ and $\widehat{\xi}^{(k')}\to\mathbf{0}$. Owing to the closedness properties of $\partial\mathcal{J}$, $\mathbf{0}\in\partial\mathcal{J}(\xi^*)$, and therefore $\xi^*\in\mathcal{S}$ is a critical point of $\mathcal{J}$.

For any point $\xi^*\in\mathcal{S}$, we have just seen that there must exist a subsequence $\left\{\xi^{(k')}\right\}$ with $\mathcal{J}(\xi^{(k')})\to\mathcal{J}(\xi^*)$ as $k\to\infty$. By the nonincreasing of $\mathcal{J}\left(\xi^{(k)}\right)$, it must satisfy

$$\lim_{k\to\infty}\mathcal{J}\left(\xi^{(k)}\right)=\inf_{k\in N}\mathcal{J}\left(\xi^{(k)}\right)=\mathcal{J}\left(\xi^*\right).$$

■

By Theorems 1-3 and the Kurdyka-Łojasiewicz property of $\mathcal{J}$, we show the sequence $\left\{\xi^{(k)}\right\}$ generated by algorithm (5) with some initial value converges to a local minima of $\mathcal{J}$.

Theorem 4: Suppose $\left\{\xi^{(k)}\right\}$ is a bounded sequence generated by the proposed alternating minimization method (5) with some initial point $\xi^{(0)}$, $\xi^{(k)}=\left(X^{(k)},u^{(k)}\right)$ and $X^{(k)}=\left(X_1^{(k)},X_2^{(k)},\cdots,X_p^{(k)}\right)$. Then, $\left\{\xi^{(k)}\right\}$ has finite length, i.e.,

$$\sum_{k=0}^{+\infty}\left\|\xi^{(k+1)}-\xi^{(k)}\right\|<+\infty,$$

and as a consequence, $\left\{\xi^{(k)}\right\}$ converges to a critical point of $\mathcal{J}$.

Proof: Since $\left\{\xi^{(k)}\right\}$ is a bounded sequence. Based on Theorem 3, there must exist a limit point $\xi^*\in\mathcal{S}$, ξ^* is a critical point of $\mathcal{J}$ and $\left\{\mathcal{J}\left(\xi^{(k)}\right)\right\}$ converges to $\mathcal{J}(\xi^*)$. As a consequence, there must exist some $k_1>0$ and for $k>k_1$, either

$$\mathcal{J}\left(\xi^{(k_1)}\right)=\mathcal{J}\left(\xi^{(k)}\right)=\mathcal{J}(\xi^*) \quad (22)$$

or

$$\mathcal{J}\left(\xi^{(k_1)}\right)>\mathcal{J}\left(\xi^{(k)}\right)>\mathcal{J}(\xi^*). \quad (23)$$

Clearly, if it is the first case (22), $\xi^{(k)}=\xi^{(k_1)}=\xi^*$ for all $k\geq k_1$ and the theorem holds certainly.

On the other hand, suppose it holds the second case (23). By Theorem 3, both the sequences $\left\{\mathcal{J}(\xi^{(k)})-\mathcal{J}(\xi^*)\right\}$ and $\left\{\left\|\xi^{(k)}-\xi^*\right\|\right\}$ admit zero as a cluster point. Then, for any $\varepsilon>0$ and $\eta>0$, there must be some $k_2\geq k_1$, and for $k\geq k_2$, it has

$$\left\|\xi^{(k)}-\xi^*\right\|<\epsilon,\quad \mathcal{J}(\xi^*)<\mathcal{J}\left(\xi^{(k)}\right)<\mathcal{J}(\xi^*)+\eta. \quad (24)$$

Denote by $\Delta\mathcal{J}\left(\xi^{(k)}\right)=\mathcal{J}\left(\xi^{(k)}\right)-\mathcal{J}(\xi^*)$,

$$0<\Delta\mathcal{J}\left(\xi^{(k)}\right)<\eta,\quad\forall\ k\geq k_2.$$

Cause ξ^* to be a critical point of $\mathcal{J}$, in the sense of the Kurdyka-Łojasiewicz property, $0<\varphi'\left(\Delta\mathcal{J}\left(\xi^{(k)}\right)\right)$ for all $k\geq k_2$. Based on (6) and φ being a concave function, for all $k\geq k_2$,

$$\frac{\varrho_{\min}}{2}\left\|\xi^{(k+1)}-\xi^{(k)}\right\|^2\leq\mathcal{J}\left(\xi^{(k)}\right)-\mathcal{J}\left(\xi^{(k+1)}\right), \quad (25)$$

and

$$\frac{\varrho_{\min}}{2}\varphi'\left(\Delta\mathcal{J}\left(\xi^{(k)}\right)\right)\left\|\xi^{(k+1)}-\xi^{(k)}\right\|^2 \leq\varphi'\left(\Delta\mathcal{J}\left(\xi^{(k)}\right)\right)\left(\mathcal{J}\left(\xi^{(k)}\right)-\mathcal{J}\left(\xi^{(k+1)}\right)\right) \leq\varphi\left(\Delta\mathcal{J}\left(\xi^{(k)}\right)\right)-\varphi\left(\Delta\mathcal{J}\left(\xi^{(k+1)}\right)\right). \quad (26)$$

With the same definition in Theorem 2, we suppose $\widehat{\xi}^{(k)}=\left(\widehat{X}_1^{(k)},\widehat{X}_2^{(k)},\cdots\widehat{X}_p^{(k)},\widehat{u}^{(k)}\right)$ to be an element of $\partial\mathcal{J}\left(\xi^{(k)}\right)$. According to the Kurdyka-Łojasiewicz property at point $\xi^{(k)}$, it holds that

$$\begin{aligned}1&\leq\varphi'\left(\Delta\mathcal{J}\left(\xi^{(k)}\right)\right)\operatorname{dist}\left(\mathbf{0},\partial\mathcal{J}\left(\xi^{(k)}\right)\right)\\&=\varphi'\left(\Delta\mathcal{J}\left(\xi^{(k)}\right)\right)\left\|\widehat{\xi}^{(k)}\right\|,\quad\forall\ k\geq k_2,\end{aligned}$$

and by (15),

$$\frac{1}{c\left\|\xi^{(k)}-\xi^{(k-1)}\right\|} \leq \frac{1}{\left\|\widehat{\xi^{(k)}}\right\|} \leq \varphi'\left(\Delta\mathcal{J}\left(\xi^{(k)}\right)\right). \quad (27)$$

Combining (26) with (27), for $k \geq k_2+1$,

$$\frac{\varrho_{\min}}{2c}\frac{\left\|\xi^{(k+1)}-\xi^{(k)}\right\|^2}{\left\|\xi^{(k)}-\xi^{(k-1)}\right\|} \leq \varphi\left(\Delta\mathcal{J}\left(\xi^{(k)}\right)\right)-\varphi\left(\Delta\mathcal{J}\left(\xi^{(k+1)}\right)\right).$$

The above inequality can be further reformed as

$$\left\|\xi^{(k+1)}-\xi^{(k)}\right\| \leq \left\|\xi^{(k)}-\xi^{(k-1)}\right\|^{\frac{1}{2}} \cdot\sqrt{\frac{2c}{\varrho_{\min}}}\left[\varphi\left(\Delta\mathcal{J}\left(\xi^{(k)}\right)\right)-\varphi\left(\Delta\mathcal{J}\left(\xi^{(k+1)}\right)\right)\right]^{\frac{1}{2}}.$$

By the inequality theory $2ab \leq a^2+b^2$,

$$2\left\|\xi^{(k+1)}-\xi^{(k)}\right\| \leq \left\|\xi^{(k)}-\xi^{(k-1)}\right\| + \frac{2c}{\varrho_{\min}}\left[\varphi\left(\Delta\mathcal{J}\left(\xi^{(k)}\right)\right)-\varphi\left(\Delta\mathcal{J}\left(\xi^{(k+1)}\right)\right)\right]. \quad (28)$$

Summing (28) for k running from $k=k_2+1$ to some K,

$$\sum_{k=k_2+1}^{K}\left\|\xi^{(k+1)}-\xi^{(k)}\right\| + \left\|\xi^{(k+1)}-\xi^{(k)}\right\| \leq \frac{2c}{\varrho_{\min}}\left[\varphi\left(\Delta\mathcal{J}\left(\xi^{(k_2+1)}\right)\right)-\varphi\left(\Delta\mathcal{J}\left(\xi^{(k+1)}\right)\right)\right] + \left\|\xi^{(k_2+1)}-\xi^{(k_2)}\right\|.$$

Therefore,

$$\sum_{k=k_2+1}^{K}\left\|\xi^{(k+1)}-\xi^{(k)}\right\| \leq \left\|\xi^{(k_2+1)}-\xi^{(k_2)}\right\| + \frac{2c}{\varrho_{\min}}\varphi\left(\Delta\mathcal{J}\left(\xi^{(k_2+1)}\right)\right). \quad (29)$$

Let $K \to \infty$, it yields that

$$\sum_{k=k_2+1}^{\infty}\left\|\xi^{(k+1)}-\xi^{(k)}\right\| \leq \left\|\xi^{(k_2+1)}-\xi^{(k_2)}\right\| + \frac{2c}{\varrho_{\min}}\varphi\left(\Delta\mathcal{J}\left(\xi^{(k_2+1)}\right)\right).$$

By (24) and (25),

$$\sum_{k=k_2+1}^{\infty}\left\|\xi^{(k+1)}-\xi^{(k)}\right\| \leq \sqrt{\frac{2}{\varrho_{\min}}\mathcal{J}\left(\xi^{(k_2)}\right)-\mathcal{J}\left(\xi^{*}\right)} + \frac{2c}{\varrho_{\min}}\varphi\left(\mathcal{J}\left(\xi^{(k_2+1)}\right)-\mathcal{J}(\xi^{*})\right), \quad (30)$$

which means

$$\sum_{k=0}^{+\infty}\left\|\xi^{(k+1)}-\xi^{(k)}\right\| < +\infty,$$

and

$$\lim_{k\to\infty}\sum_{l=k}^{\infty}\left\|\xi^{(l+1)}-\xi^{(l)}\right\| = 0.$$

Clearly, $\left\{\xi^{(k)}\right\}$ is a Cauchy sequence and convergent sequence. According to Theorem 3, $\left\{\xi^{(k)}\right\}$ converges to a critical point of $\mathcal{J}$ and the theorem is proved. ■

V. Numerical Results

In this section, numerical experimental results are illustrated to demonstrate the effectiveness of the proposed method. The constantly used 256-by-256 images Cameraman, Butterfly, Light, House, Zebra, Mickey; and 512-by-512 images Bridge, Boat, Barbara, Hill, Man, Fence are adopted in our experiments. These original tested images are shown in Fig. 1. The degraded images are obtained by image degradation model (1), which are the clean images down-sampled by different partial down-sampling operators without additive white Gaussian noise. A text pixels missing operator and random 50%, 60%, 70% and 80% pixels missing operators are respectively considered in the experiments.

Algorithm 1 Alternating Proximal Gradient Method for Image Inpainting

1. Input observed image g, initialize parameters s, t, λ, $\alpha_1, \alpha_2, \cdots, \alpha_p, \beta$ and the maximum iteration number K_0, set iteration index $k=1$.
2. Initialize $u^{(0)}$ and determine matching patch extracting matrices $R_1, R_2, \cdots, R_p$ by conducting image block matching schemes on $u^{(0)}$, set $X_i^{(0)} = R_i u^{(0)}$ for $i = 1, 2, \cdots, p$.
3. **When** $k < K$, **do**

1) Update matching patch extracting matrices R_1, R_2, $\cdots$, R_p by conducting image block matching schemes on $u^{(k-1)}$;

2) **For** $i = 1, 2, \cdots, p$, conduct SVD

$$\left[U_i^{(k)}, \Sigma_i^{(k)}, V_i^{(k)}\right] = \left(\frac{\varrho_i}{\alpha_i}X_i^{(k-1)} + \frac{\lambda}{\alpha_i}\mathcal{M}R_i u^{(k-1)}\right),$$

and update

$$X_i^{(k)} = U_i^{(k-1)}\mathcal{D}_{\frac{\omega_i}{\alpha_i}}\left(\Sigma_i^{(k-1)}\right)\left(V_i^{(k-1)}\right)^T,$$

End for and output

$$X^{(k)} = \left(X_1^{(k)}, X_2^{(k)}, \cdots, X_p^{(k)}\right);$$

3) Update

$$u^{(k)} = A^{-1}\left(H^T g + \varrho W u^{(k-1)} + \lambda\sum_{i=1}^{p}R_i^T\mathcal{V}X_i^{(k)}\right);$$

4) Compute

$$\mathrm{Tol} = \frac{||u^{(k)}-u^{(k-1)}||_2}{||u^{(k)}||_2},$$

if $\mathrm{Tol} < 10^{-4}$, stop; else $k = k+1$, and go back to step 3;

4. **End for** and output $X^{(k)}$, $u^{(k)}$.

To evaluate the performances of the proposed method, six current state-of-the-art methods are also conducted in the experiments as compared methods. They are the exemplar-based methods named by "EPLL" [16] and "IPPO" [51]; multi-scale weighted nuclear norm minimization method named by "WNNM" [35]; group

sparsity and WSNM-based low-rank method named by "WSNM" [42]; customized low-rank prior-based method named by "CLRP" [52]; proximal alternating and matrix rank minimization-based method named by "PARM" [53]. The proposed method is denoted as "RM-APG" and its details are concluded in Algorithm 1. The peak signal-to-noise ratio (PSNR, peak signal-to-noise ratio) and structure similarity index measure (SSIM, structure similarity index measure) [54] are used to measure the qualities of the recovered images in all experiments. PSNR is defined as

$$\mathrm{PSNR} = 10\log 10\frac{mn\cdot|\max(u)-\min(u)|^2}{\|\hat{u}-u\|_2^2}(\mathrm{dB}),$$

here u is the column stacked mn-by-1 noise-free image and $\hat{u}$ is its restored version. SSIM is a full reference metric and it can efficiently measure the similarity between two images.

The parameters in proposed "APG-RM" method are set as follows. The size of each reference patch is 8×8 and the number of similar image patches to each reference patch is set to be 60. The size of nonlocal window within which the similar patches are searched is set to be 60×60. Since missing pixels in degraded image may influence the matching of similar patches. We utilize a simple interpolation operation to fill the missing pixels to get an initial guess $u^{(0)}$, and then conduct the block matching schemes on $u^{(0)}$ to get the matching patch extracting matrices $R_1, R_2, \cdots, R_p$. For $i = 1, 2, \cdots, p$, each $X_i^{(0)}$ is consequently set to be $R_i u^{(0)}$, and the parameter ω_i is set to be $2\sqrt{2t}\delta_i^2$, where δ_i is the standard deviation of the noise in corresponding degraded low-rank matrix and can be estimated by approaches introduced in literatures [28], [31]. The parameter λ is selected in interval $[0.0001, 0.1]$. The more seriously degraded the image, the smaller the parameter λ is selected. $\alpha_1, \alpha_2, \cdots, \alpha_p, \beta$ are set to be $\lambda + 10^{-5}$.

$$\frac{\left\|u^{(k+1)}-u^{(k)}\right\|_2}{\left\|u^{(k+1)}\right\|_2} < 10^{-4}$$

is adopted as the stopping criterion in "APG-RM" method and the maximum iteration number is set to be 600. The required parameters in the six compared methods are set as those suggested by their authors except for which to achieve the best recovery results.

The PSNRs and SSIMs of all recovered images by different methods for the text and random 50%, 60%, 70%, 80% pixels missing degradation experiments are listed in Table I-Table V, respectively. We can see obviously that the nonlocal low-rank minimization methods "PARM", "WSNM" and proposed method "APG-RM" obtain much better recovered measure quantities than the other methods. The best PSNRs and SSIMs for each image restoration in these tables are shown in boldface, and they are almost all obtained by our proposed "APG-RM" methods. To further evaluate the performances of these methods, the average PSNRs, SSIMs and TIMEs of all recovered images in Table I-Table V are listed in Table VI, where "TIME" denotes the average consumed time in seconds of all recovered images by each method. In Table VI, the best average PSNRs and SSIMs are also shown in boldface and they are all obtained by the proposed "APG-RM" methods. To make a more intuitive comparison of the average PSNRs and SSIMs, the

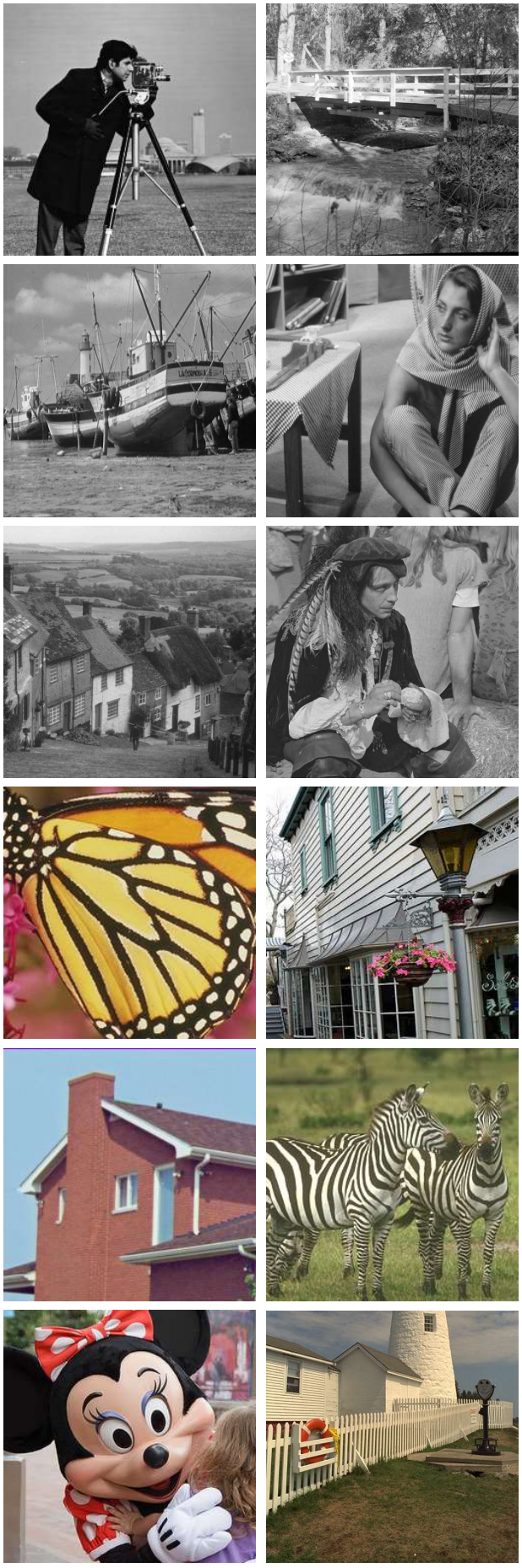

Fig. 1. Original tested images, from left to right, the first column: Cameraman, Boat, Hill, Butterfly, House and Mickey; the second column: Bridge, Barbara, Man, Light, Zebra and Fence; respectively.

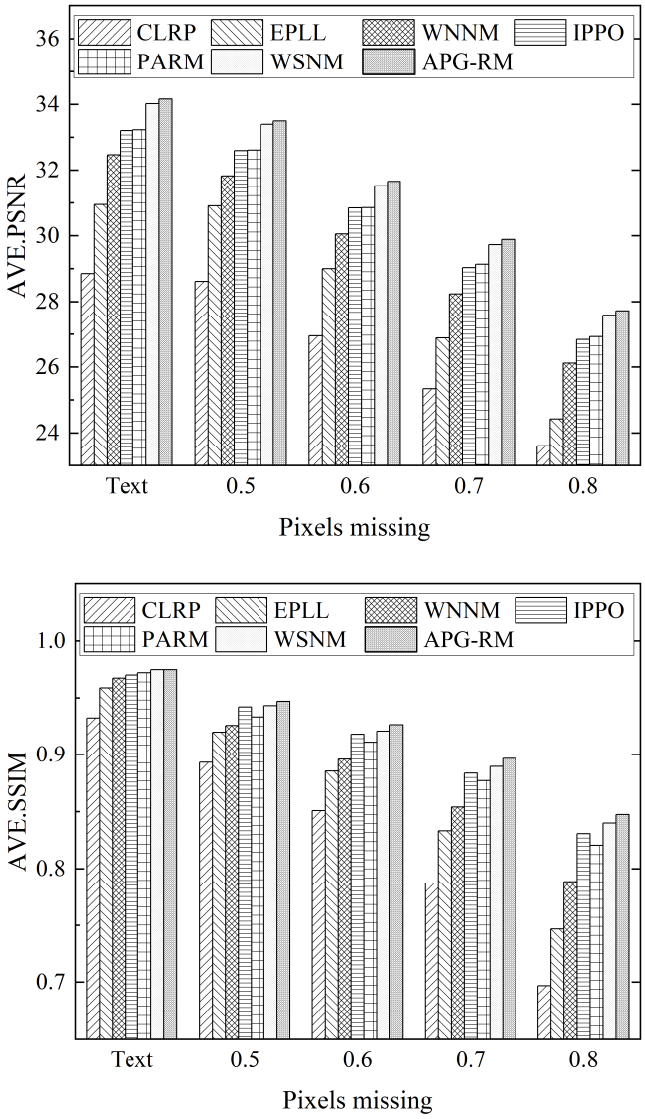

Fig. 2. Histograms of average PSNRs and SSIMs in Table VI.

histograms of them are shown in Fig. 2.

The computation complexity of "APG-RM" method is very similar to that of "PARM" method, except for the solving of linear system (5) which can be solved by a direct inverse operation instead of the conjugate gradient method in "PARM", see, [32], [53]. Moreover, the complexity of our proposed method compared with the other methods can be investigated by the average consumed time listed in Table VI. In Table VI, it can be seen that the nonlocal low-rank minimization methods "WNNM", "PARM", "WSNM" and "APG-RM" are much more time consuming. This is because the patch matching matrix extraction and the SVD decomposition-based low-rank matrix minimization operations in these methods are quite time consuming and much more round of iterations of them are also needed. The "WSNM" and "APG-RM" are the most time consuming, because the image block matching schemes are conducted in each iteration of these methods to achieve the image restoration qualities.

Due to space limitation considerations, we show the recovered House images for Text pixels missing degradation, Butterfly images for random 50% pixels missing degradation, Boat images for random 60% pixels missing degradation, Barbara images for random 70% pixels missing degradation and Fence images for random 80% pixels missing degradation to illustrate the visual effects in Fig. 3-Fig. 7. In each of these figures, from left to right, the first line are the pixels missing degraded image and recovered images by methods "CLRP", "EPLL" and "WNNM", the second line are the recovered images by methods "IPPO", "PARM", "WSNM" and "APG-RM", respectively. It can be seen from Fig. 3-Fig. 7 that the visual effects of the recovered images by different methods are consistent with the recovered quantity measures in Tables I-V, respectively. The "IPPO", "PARM", "WSNM" and proposed "APG-RM" methods recovered images have much better visual effects than that of the "CLRP", "EPLL" and "WNNM" methods. To see more clearly the recovered visual effects, we extract one small block encircled by white square box and show it in a larger block encircled by a white square box in each image in these figures. From enlarged blocks in Fig. 3-Fig. 7, it can be seen that "WSNM" and the proposed "APG-RM" methods recovered images have obviously better visual effects than those of "IPPO" and "PARM" methods, and the enlarged blocks in "APG-RM" method recovered images show slightly better visual effects than that of "WSNM" method recovered images. For instance, the enlarged blocks in "APG-RM" method recovered Boat image in Fig. 5 and Fence image in Fig. 7 are much more clearer than that of "WSNM" recovered images. Since "WNNM", "IPPO", "PARM" and "WSNM" methods are all current state-of-the-art methods for image inpainting, the numerical results in these tables and figures illustrate that the proposed "APG-RM" methods can well complete with these methods.

VI. Conclusion

In this paper, a novel nonlocal low-rank minimization-based regularization method is proposed for image inpainting. The regularization model is developed by a direct rank minimization-based regularization term and a L_2-norm fidelity term. An alternating proximal gradient algorithm is designed to solve the nonconvex regularization model, and the convergence of the algorithm is analyzed and proved by the famous Kurdyka-Łojasiewicz property. Numerical experiments demonstrate that the proposed method is comparable to the current state-of-the-art nonlocal low-rank minimization methods for image inpainting.

References

[1] J. Jam, C. Kendrick, K. Walker, V. Drouard, J. G. S. Hsu and M. H. Yap, "A comprehensive review of past and present image inpainting methods," *Computer vision and image understanding*, vol. 203, 103147, 2021.

[2] Q. Peng and W. Huang, "An image inpainting algorithm using exemplar matching and low-rank sparse prior," *Inverse Problems*, vol. 40, no. 1, 015002, 2023.

[3] G. Cristóbal, P. Schelkens and H. Thienpont, *Optical and Digital Image Processing*, John Wiley & Sons, 2013.

[4] B. K. Gunturk and X. Li, *Image Restoration*, CRC Press, 2018.

[5] F. Yao, "Damaged region filling by improved criminisi image inpainting algorithm for thangka," *Cluster Comput.*, vol. 22, pp. 13683-13691, 2019.

[6] Z. Wan, B. Zhang, D. Chen, P. Zhang, D. Chen, J. Liao and F. Wen, "Bringing old photos back to life," in *CVPR 2020*, pp. 2747-2757.

TABLE I
RECOVERED MEASURES FOR TEXT PIXELS MISSING.

Images	Measures	CLRP	EPLL	WNNM	IPPO	PARM	WSNM	APG-RM
C.man	PSNR	28.61	30.10	30.77	32.04	30.72	31.51	**32.07**
	SSIM	0.9410	0.9592	0.9651	0.9692	0.9654	0.9675	**0.9690**
B.fly	PSNR	28.72	30.58	33.77	33.98	34.49	**34.85**	34.81
	SSIM	0.9543	0.9709	0.9840	0.9699	0.9862	**0.9872**	0.9864
Light	PSNR	24.84	27.29	29.13	29.92	29.53	30.09	**30.35**
	SSIM	0.9083	0.9436	0.9605	0.9675	0.9670	0.9697	**0.9715**
House	PSNR	35.40	38.44	40.42	41.06	42.03	42.24	**42.48**
	SSIM	0.9281	0.9715	0.9783	0.9850	0.9822	0.9828	**0.9846**
Zebra	PSNR	25.10	27.75	27.62	28.19	28.56	29.99	**30.18**
	SSIM	0.9191	0.9445	0.9466	0.9516	0.9557	0.9587	**0.9599**
Mickey	PSNR	30.46	31.53	33.12	34.04	34.07	35.07	**35.10**
	SSIM	0.9438	0.9639	0.9700	0.9778	0.9767	0.9777	**0.9788**

TABLE II
RECOVERED MEASURES FOR RANDOM 50% PIXELS MISSING.

Images	Measures	CLRP	EPLL	WNNM	IPPO	PARM	WSNM	APG-RM
C.man	PSNR	27.73	29.11	30.31	30.74	30.05	30.85	**31.00**
	SSIM	0.9151	0.9271	0.9316	0.9397	0.9368	0.9404	**0.9423**
B.fly	PSNR	28.76	30.06	32.17	31.73	32.84	33.00	**33.12**
	SSIM	0.9488	0.9572	0.9673	0.9699	0.9158	0.9708	**0.9759**
Light	PSNR	21.71	23.93	26.60	26.74	26.53	27.08	**27.18**
	SSIM	0.8206	0.8847	0.9287	0.9355	0.9377	0.9404	**0.9443**
House	PSNR	34.39	37.47	38.70	39.98	39.76	41.10	**41.48**
	SSIM	0.9118	0.9450	0.9555	0.9735	0.9597	0.9649	**0.9750**
Zebra	PSNR	24.20	26.98	27.45	28.48	27.22	28.21	**28.83**
	SSIM	0.8781	0.9101	0.9117	0.9306	0.9212	0.9294	**0.9370**
Mickey	PSNR	29.17	30.33	31.77	32.79	33.15	33.70	**33.94**
	SSIM	0.9276	0.9383	0.9429	0.9612	0.9596	0.9603	**0.9650**
Bridge	PSNR	27.38	28.24	28.24	28.40	28.25	28.27	**28.45**
	SSIM	0.8554	0.8749	0.8691	0.8884	0.8864	0.8900	**0.8932**
Boats	PSNR	30.84	33.21	33.35	34.16	34.67	35.21	**35.30**
	SSIM	0.8959	0.9202	0.9157	0.9349	0.9313	0.9408	**0.9428**
Barbara	PSNR	26.34	32.09	33.63	35.86	36.05	**38.50**	38.49
	SSIM	0.8757	0.9438	0.9562	0.9701	0.9693	**0.9773**	0.9763
Hill	PSNR	32.35	33.72	33.67	34.69	34.89	35.17	**35.40**
	SSIM	0.8996	0.9110	0.9085	0.9314	0.9270	0.9305	**0.9372**
Man	PSNR	31.95	33.06	33.03	34.05	34.09	34.15	**34.53**
	SSIM	0.9178	0.9241	0.9200	0.9467	0.9388	0.9404	**0.9488**
Fence	PSNR	28.57	32.69	32.99	33.53	33.84	**34.34**	34.32
	SSIM	0.8736	0.9030	0.9020	0.9219	0.9158	0.9205	**0.9258**

[7] Y. G. Wang, L. Wang and Y. X. Geng, "Research on medical image classification based on triple fusion attention," *Engineering Letters*, vol. 33, no. 1, pp. 124-131, 2025.

[8] H.-Y. Yan, Y.-P. Liu, H.-X. Wang and H. Chen, "Rank minimization method for speckle noise removal in ultrasound images," *Engineering Letters*, vol. 33, no. 6, pp. 2228-2242, 2025.

[9] X. Zhang and JWL Wan, "Image restoration of medical images with streaking artifacts by Euler's elastica inpainting," in *ISBI 2017*, pp. 235-239.

[10] D. Yi, Z. You and W. Zhang, "Image enhancement CHPSO processing technology based on improved particle swarm optimization algorithm," *IAENG International Journal of Computer Science*, vol. 52, no. 1, pp. 130-142, 2025.

[11] Y.-T. Wang, X.-L. Zhao, T.-X. Jiang, L.-J. Deng, Y. Chang and T.-Z. Huang, "Rain streaks removal for single image via kernel-guided convolutional neural network," *IEEE Trans. Neural Netw. Learn. Syst.*, vol. 32, pp. 3664-3676, 2020.

[12] S. Ge, D. Liu, X. Shi, X. Zhao, X. Wang and J. Fan, "Semantic segmentation of remote sensing images based on filtered hybrid attention mechanisms," *Engineering Letters*, vol. 33, no. 1, pp.80-89, 2025.

[13] S. Guastavino and F. Benvenuto, "A mathematical model for image saturation with an application to the restoration of solar images via adaptive sparse deconvolution," *Inverse Problems*, vol. 37, 015010, 2020.

[14] M. Ma, "Color image restoration via quaternion-based hybrid regularization method," *IAENG International Journal of Applied Mathematics*, vol. 54, no. 11, pp. 2176-2182, 2024.

[15] A. K. Awasthi, Y. Kumar and H. Abdullahi, "Optimizing conjugate gradient directions for image deblurring in compressed sensing: a hybridized approach," *IAENG International Journal of Applied Mathematics*, vol. 54, no. 11, pp. 2500-2511, 2024.

[16] D. Zoran and Y. Weiss, "From learning models of natural image patches to whole image restoration," in *ICCV 2011*, pp. 479-486.

[17] M. Li, Y. Huang and Y. Wen, "A Total Variation Based Method for Multivariate Time Series Segmentation," *Adv. Appl. Math. Mech.*, vol. 15, no. 2, pp. 300-321, 2023.

[18] M. Bertalmio, G. Sapiro, V. Caselles and C. Ballester, "Image inpainting," in *Proc. 27th Annual Conf. on Computer Graphics and Interactive Techniques 2000*, pp. 417-424.

TABLE III
RECOVERED MEASURES FOR RANDOM 60% PIXELS MISSING.

Images	Measures	CLRP	EPLL	WNNM	IPPO	PARM	WSNM	APG-RM
C.man	PSNR	26.10	27.41	28.43	28.70	28.59	28.90	**29.03**
	SSIM	0.8740	0.9002	0.9069	0.9161	0.9169	0.9210	**0.9236**
B.fly	PSNR	26.70	27.92	30.28	29.88	31.00	31.20	**31.36**
	SSIM	0.9199	0.9354	0.9520	0.9567	0.9607	0.9634	**0.9666**
Light	PSNR	20.17	22.27	24.42	25.12	24.77	25.06	**25.29**
	SSIM	0.7359	0.8270	0.8867	0.9055	0.9070	0.9113	**0.9178**
House	PSNR	31.93	35.16	37.10	38.23	38.05	39.35	**39.65**
	SSIM	0.9086	0.9280	0.9400	0.9625	0.9444	0.9572	**0.9663**
Zebra	PSNR	22.56	24.97	25.60	26.77	25.66	26.46	**26.66**
	SSIM	0.8247	0.8655	0.8731	0.8997	0.8858	0.9005	**0.9060**
Mickey	PSNR	27.51	28.47	29.62	30.74	30.70	31.32	**31.34**
	SSIM	0.8913	0.9095	0.9175	0.9423	0.9363	0.9480	**0.9483**
Bridge	PSNR	26.00	26.80	26.91	26.98	26.96	27.02	**27.03**
	SSIM	0.7994	0.8246	0.8201	0.8446	0.8407	**0.8561**	0.8539
Boats	PSNR	29.11	31.21	31.60	32.34	32.70	33.34	**33.44**
	SSIM	0.8581	0.8898	0.8850	0.9100	0.9025	0.9206	0.9221
Barbara	PSNR	25.35	29.60	31.68	34.15	34.33	**36.81**	36.79
	SSIM	0.8352	0.9115	0.9360	0.9580	0.9552	0.9687	**0.9688**
Hill	PSNR	30.80	32.09	32.08	32.96	33.14	33.72	**33.85**
	SSIM	0.8612	0.8764	0.8735	0.9047	0.8947	0.9058	**0.9158**
Man	PSNR	30.33	31.31	31.48	32.37	32.19	**32.82**	32.78
	SSIM	0.8823	0.8927	0.8901	0.9235	0.9079	0.9282	**0.9287**
Fence	PSNR	26.89	30.80	31.44	31.92	32.20	32.73	**32.76**
	SSIM	0.8217	0.8653	0.8695	0.8923	0.8803	0.8996	**0.9004**

TABLE IV
RECOVERED MEASURES FOR RANDOM 70% PIXELS MISSING.

Images	Measures	CLRP	EPLL	WNNM	IPPO	PARM	WSNM	APG-RM
C.man	PSNR	24.57	25.46	26.69	26.89	27.18	27.56	**27.79**
	SSIM	0.8069	0.8597	0.8737	0.8843	0.8892	0.8919	**0.8987**
B.fly	PSNR	24.48	25.16	28.30	27.63	28.97	**29.28**	29.20
	SSIM	0.8685	0.8919	0.9306	0.9357	0.9439	**0.9514**	0.9512
Light	PSNR	19.29	20.57	22.01	23.49	22.70	23.79	**23.94**
	SSIM	0.6598	0.7349	0.8120	0.8612	0.8605	0.8807	**0.8874**
House	PSNR	30.14	31.92	35.46	36.62	36.62	37.00	37.28
	SSIM	0.8652	0.9044	0.9221	0.9485	0.9284	0.9402	**0.9466**
Zebra	PSNR	20.82	22.86	23.42	24.77	23.41	24.52	**24.70**
	SSIM	0.7455	0.7964	0.8155	0.8498	0.8340	0.8503	**0.8632**
Mickey	PSNR	25.96	26.59	27.84	28.61	28.79	**29.25**	29.18
	SSIM	0.8396	0.8680	0.8845	0.9149	0.9099	**0.9266**	0.9246
Bridge	PSNR	23.79	25.37	25.63	25.56	25.61	25.69	**25.76**
	SSIM	0.6924	0.7550	0.7557	0.7840	0.7826	0.7999	**0.8013**
Boats	PSNR	27.33	29.02	29.70	30.46	30.82	31.20	**31.31**
	SSIM	0.8028	0.8435	0.8436	0.8758	0.8679	0.8808	**0.8885**
Barbara	PSNR	24.48	27.13	29.36	32.19	32.54	34.66	**34.87**
	SSIM	0.7807	0.8567	0.8997	0.9393	0.9362	0.9446	**0.9566**
Hill	PSNR	29.27	30.37	30.54	31.28	31.52	32.06	**32.22**
	SSIM	0.8075	0.8280	0.8298	0.8677	0.8560	0.8756	**0.8828**
Man	PSNR	28.70	29.47	30.01	30.71	30.63	**31.16**	31.13
	SSIM	0.8303	0.8473	0.8526	0.8920	0.8736	0.8944	**0.8973**
Fence	PSNR	25.32	28.72	29.89	30.20	30.80	31.02	**31.33**
	SSIM	0.7500	0.8132	0.8285	0.8528	0.8428	0.8481	**0.8621**

TABLE V
RECOVERED MEASURES FOR RANDOM 80% PIXELS MISSING.

Images	Measures	CLRP	EPLL	WNNM	IPPO	PARM	WSNM	APG-RM
C.man	PSNR	23.02	23.19	24.60	24.89	24.72	25.05	**25.09**
	SSIM	0.7156	0.7936	0.8243	0.8419	0.8396	0.8402	**0.8486**
B.fly	PSNR	21.52	21.69	25.65	25.11	26.47	26.23	**26.43**
	SSIM	0.7742	0.7948	0.8924	0.8994	0.9141	0.9201	**0.9233**
Light	PSNR	18.10	18.96	19.67	21.50	19.91	22.04	**22.12**
	SSIM	0.5386	0.6029	0.6766	0.7827	0.7417	0.8204	**0.8318**
House	PSNR	27.68	28.71	33.18	33.67	34.82	35.06	**35.21**
	SSIM	0.7871	0.8639	0.8944	0.9218	0.9074	0.9188	**0.9244**
Zebra	PSNR	19.17	20.52	21.51	22.01	21.44	22.58	**22.70**
	SSIM	0.6316	0.6827	0.7359	0.7742	0.7602	0.7903	**0.7938**
Mickey	PSNR	24.10	24.09	25.62	26.36	26.28	**26.85**	26.82
	SSIM	0.7590	0.7910	0.8301	0.8687	0.8603	**0.8815**	0.8813
Bridge	PSNR	22.66	23.45	24.23	24.11	24.13	24.16	**24.24**
	SSIM	0.6074	0.6422	0.6684	0.6995	0.7008	0.7119	**0.7213**
Boats	PSNR	25.35	26.47	27.69	28.25	28.59	28.72	**28.92**
	SSIM	0.7159	0.7655	0.7840	0.8223	0.8138	0.8306	**0.8337**
Barbara	PSNR	23.55	24.74	26.38	29.71	29.59	32.19	**32.37**
	SSIM	0.7017	0.7677	0.8209	0.9045	0.8983	0.9302	**0.9343**
Hill	PSNR	27.58	28.22	28.78	29.43	29.45	30.01	**30.10**
	SSIM	0.7299	0.7531	0.7690	0.8137	0.7951	0.8241	**0.8269**
Man	PSNR	26.86	27.13	28.32	28.80	28.83	29.02	**29.14**
	SSIM	0.7485	0.7735	0.7991	0.8412	0.8232	0.8346	**0.8446**
Fence	PSNR	23.76	25.97	27.76	28.40	28.89	29.43	**29.50**
	SSIM	0.6534	0.7301	0.7683	0.8001	0.7925	0.8006	**0.8075**

TABLE VI
THE AVERAGE RECOVERED MEASURES.

Pixels missing	Measures	Methods						
		CLRP	EPLL	WNNM	IPPO	PARM	WSNM	APG-RM
Text	PSNR	28.855	30.948	32.472	33.205	33.233	34.032	**34.165**
	SSIM	0.9324	0.9589	0.9674	0.9702	0.9722	0.9748	**0.9750**
	TIME	**1.04**	31.27	604.07	116.32	831.23	2712.22	2507.11
50%	PSNR	28.616	30.908	31.826	32.596	32.612	33.400	**33.503**
	SSIM	0.8933	0.9200	0.9258	0.9420	0.9333	0.9431	**0.9470**
	TIME	**6.02**	67.76	1003.11	712.62	498.62	3546.87	3696.78
60%	PSNR	26.954	29.001	30.053	30.847	30.858	31.531	**31.665**
	SSIM	0.8510	0.8855	0.8959	0.9180	0.9110	0.9209	**0.9265**
	TIME	**4.78**	57.72	1059.91	568.36	722.06	2567.23	2700.72
70%	PSNR	25.346	26.887	28.238	29.034	29.133	29.733	**29.893**
	SSIM	0.7874	0.8333	0.8540	0.8838	0.8771	0.8895	**0.8967**
	TIME	**3.49**	57.75	1036.54	405.78	909.96	1892.10	1609.27
80%	PSNR	23.613	24.428	26.116	26.837	26.927	27.582	**27.720**
	SSIM	0.6969	0.7468	0.7886	0.8308	0.8206	0.8400	**0.8476**
	TIME	**3.91**	57.71	1027.13	294.57	1047.84	1984.83	1787.27

[19] J. Shen and T. F. Chan, "Mathematical models for local nontexture inpaintings," *SIAM J. Appl. Math.*, vol. 62, pp. 1019-1043, 2002.

[20] A. A. Efros and T. K. Leung "Texture synthesis by non-parametric sampling," in *ICCV 1999*, pp. 1033-1038.

[21] A. Buades, B. Coll and J. M. Morel, "A non-local algorithm for image denoising," in *CVPR 2005*.

[22] M. Ghorai, S. Samanta, S. Mandal and B. Chanda, "Multiple pyramids based image inpainting using local patch statistics and steering kernel feature," *IEEE Trans. Image Process.*, vol. 28, pp. 5495-509, 2019.

[23] M. Elad and M. Aharon, "Image denoising via sparse and redundant representations over learned dictionaries," *IEEE Trans. Image Process.*, vol. 15, no. 12, pp. 3736-3745, 2006.

[24] J. Mairal, M. Elad and G. Sapiro, "Sparse representation for color image restoration," *IEEE Trans. Image Process.*, vol. 17, no. 1, pp. 53-69, 2008.

[25] B. Shen, W. Hu, Y. Zhang and Y. J. Zhang, "Image inpainting via sparse representation," in *2009 IEEE International Conference on Acoustics, Speech and Signal Processing*, pp. 697-700.

[26] J. Zhang, D. Zhao and W. Gao, "Group-based sparse representation for image restoration," *IEEE Trans. Image Process.*, vol. 23, no. 8, pp. 3336-3351, 2014.

[27] H. Ji, C. Liu, Z. Shen and Y. Xu, "Robust video denoising using low rank matrix completion," in *CVPR 2010*, pp. 1791–1798.

[28] W. Dong, G. Shi and X. Li, "Nonlocal image restoration with bilateral variance estimation: a low-rank approach," *IEEE Trans. Image Process.*, vol. 22, no. 2, pp. 700-711, 2013.

[29] J. Cai, E. J. Cands and Z. Shen, "A singular value thresholding algorithm for matrix completion," *SIAM J. Optim*, vol. 20, no. 4, pp.

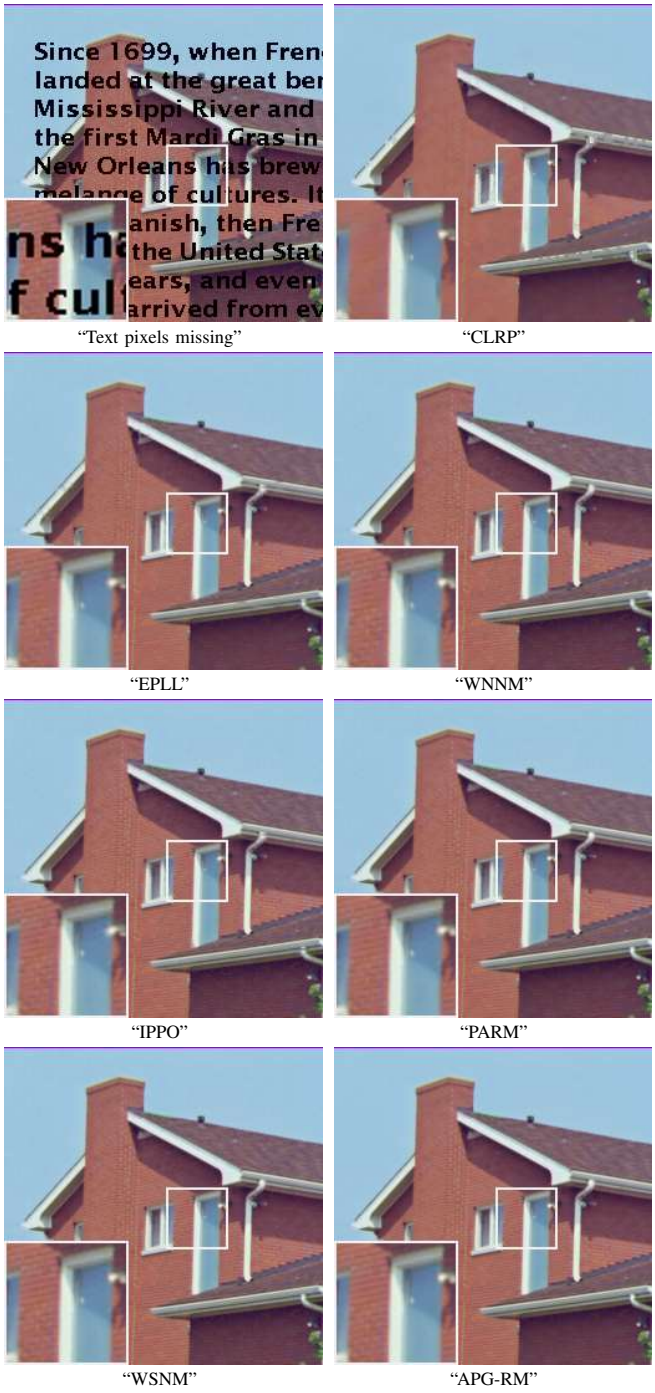

Fig. 3. Experimental results of House image for text pixels missing degradation. From up to down, the first line: the degraded image and its recovered image by “CLRP” method; the second to forth lines: the recovered images by methods “EPLL” and “WNNM”, “IPPO” and “PARM”, “WSNM” and “APG-RM”, respectively.

Fig. 4. Experimental results of Butterfly image for text pixels missing degradation. From up to down, the first line: the degraded image and its recovered image by “CLRP” method; the second to forth lines: the recovered images by methods “EPLL” and “WNNM”, “IPPO” and “PARM”, “WSNM” and “APG-RM”, respectively.

1956–1982, 2010.

[30] M. Fazel, H. Hindi and S. P. Boyd, “A rank minimization heuristic with application to minimum order system approximation,” in *Proceedings of the American Control Conference 2001*, pp. 4734–4739.

[31] S. Gu, L. Zhang, W. Zuo, and X. Feng, “Weighted nuclear norm minimization with application to image denoising,” in *CVPR 2014*, pp. 2862–2867.

[32] Y.-M. Huang and H.-Y. Yan, “Weighted nuclear norm minimization based-regularization method for image restoration,” *Commun. Appl. Math Comput.*, vol. 3, no. 3, pp. 371–389, 2021.

[33] X. Lv and F. Li, “A Decoupled method for image inpainting with patch-based low rank regularization,” *Applied Mathematics and Computation*, vol. 314, pp. 334–348, 2017.

[34] X. Lv and F. Li, “An iterative decoupled method with weighted nuclear norm minimization for image restoration,” *Int. J. Comput. Math.*, vol. 97, no. 3, pp. 602–623, 2020.

[35] N. Yair and T. Michaeli, “Multi-scale weighted nuclear norm image restoration,” in *CVPR*, pp. 3165–3174, 2018.

[36] H.-Y. Yan and Z. Zheng, “Image cartoon-texture decomposition by a generalized non-convex low-rank minimization method,” *Journal of the Franklin Institute*, vol. 361, no. 2, pp. 796–815, 2024.

[37] F. Nie, H. Wang, H. Huang and C. Ding, “Joint schatten p-norm and p-norm robust matrix completion for missing value recovery,” *Knowledge and Information Systems*, vol. 42, no. 3, pp. 525–544, 2015.

[38] Y. Xie, S. Gu, Y. Liu, W.Zuo, W. Zhang and L. Zhang, “Weighted schatten p-norm minimization for image denoising and background subtraction,” *IEEE Trans. Image Process.*, vol. 25, no. 10, pp. 4842–

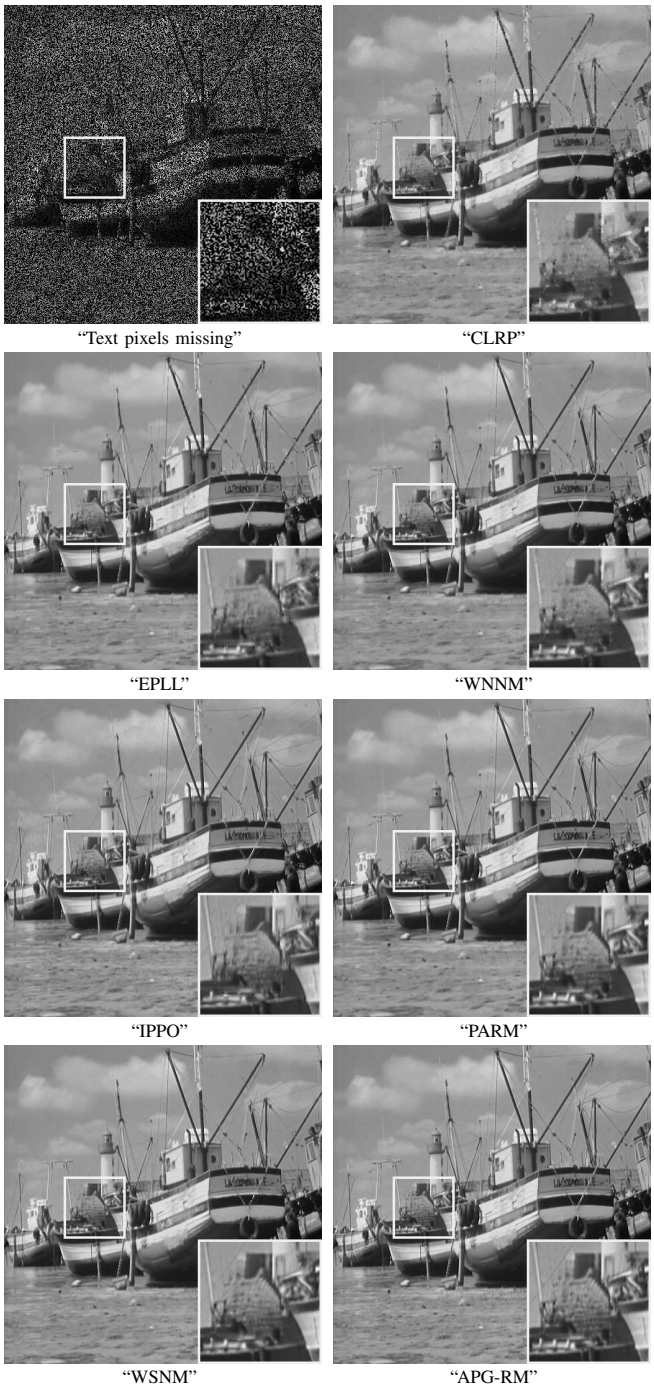

Fig. 5. Experimental results of Boat image for text pixels missing degradation. From up to down, the first line: the degraded image and its recovered image by "CLRP" method; the second to forth lines: the recovered images by methods "EPLL" and "WNNM", "IPPO" and "PARM", "WSNM" and "APG-RM", respectively.

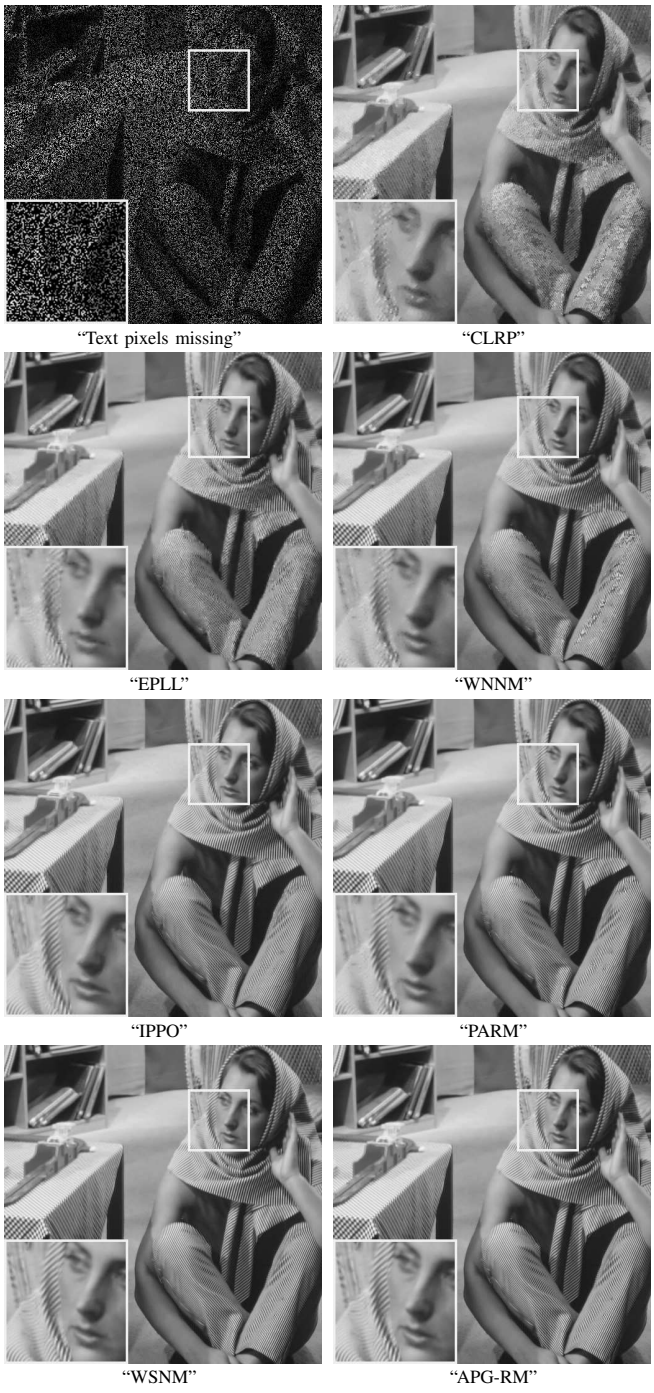

Fig. 6. Experimental results of Barbara image for text pixels missing degradation. From up to down, the first line: the degraded image and its recovered image by "CLRP" method; the second to forth lines: the recovered images by methods "EPLL" and "WNNM", "IPPO" and "PARM", "WSNM" and "APG-RM", respectively.

4857, 2016.

[39] Y. Hu, D. Zhang, J. Ye, X. Li and X. He, "Fast and accurate matrix completion via truncated nuclear norm regularization," *IEEE Trans. Pattern Anal. Mach. Intell.*, vol. 35, pp. 2117–2130, 2012.

[40] T. Geng, G. Sun, Y. Xu and J. He, "Truncated nuclear norm minimization based group sparse representation for image restoration," *SIAM J. Imag. Sci.*, vol. 11, no. 3, pp. 1878-1897, 2018.

[41] Z. Zha, X. Yuan, B. Wen, J. Zhou, J. Zhang and C. Zhu, "A benchmark for sparse coding: when group sparsity meets rank minimization," *IEEE Trans. Image Process.*, vol. 29, pp. 5094–5109, 2020.

[42] Z. Zha, B. Wen, X. Yuan, J. Zhou and C. Zhu, Image restoration via reconciliation of group sparsity and low-rank models," *IEEE Trans. Image Process.*, vol. 30, pp. 5223–5238, 2021.

[43] Y.-M.Huang, H.-Y. Yan, Y.-W. Wen and X. Yang, "Rank minimization with applications to image noise removal," *Inform. Sciences*, vol. 429, pp. 147–163, 2018.

[44] B. Mordukhovich, *Variational Analysis and Generalized Differentiation. I. Basic Theory*, Grundlehren der Mathematischen Wissenschaften, Springer-Verlag, Berlin, 2006.

[45] J. Bolte, A. Daniilidis and A. Lewis, "The Łojasiewicz inequality for nonsmooth subanalytic functions with applications to subgradient dynamical systems," *SIAM J. Optim.*, vol. 17, no. 4, pp. 1205-1223, 2006.

[46] H. Attouch, J. Bolte, P. Redont and A. Soubeyran, "Proximal alternating minimization and projection methods for nonconvex problems: an approach based on the Kurdyka-Łojasiewicz inequality," *Math. Oper. Res.*, vol. 35, no. 2, pp. 438–457, 2010.

[47] H. Attouch, J. Bolte and B. F. Svaiter, "Convergence of descent

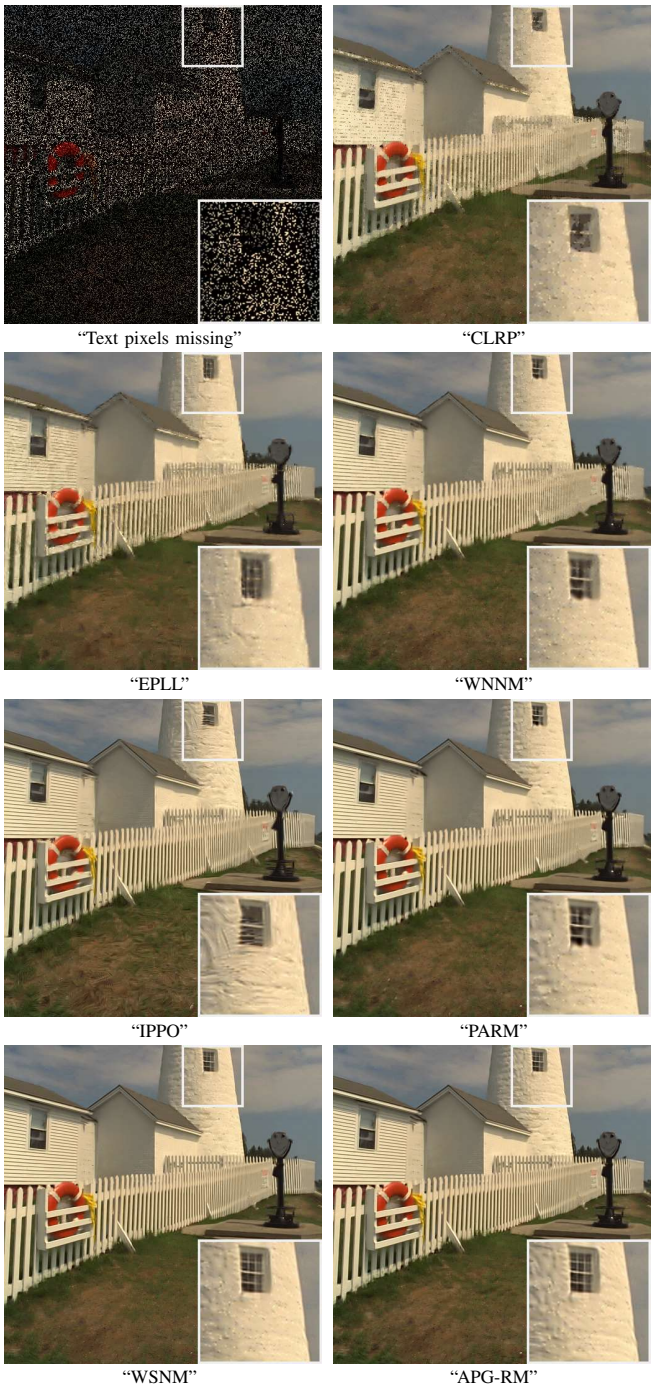

Fig. 7. Experimental results of Fence image for text pixels missing degradation. From up to down, the first line: the degraded image and its recovered image by "CLRP" method; the second to forth lines: the recovered images by methods "EPLL" and "WNNM", "IPPO" and "PARM", "WSNM" and "APG-RM", respectively.

methods for semi-algebraic and tame problems: proximal algorithms, forward-backward splitting, and regularized Gauss-Seidel methods," *Math. Program.*, vol. 137, pp. 91-29, 2013.

[48] J. Bolte, S. Sabach and M. Teboulle, "Proximal alternating linearized minimization for nonconvex and nonsmooth problems," *Math. Program.*, vol. 146, no. 1, pp. 459-494, 2013.

[49] J. Bochnak, M. Coste and M. F. Roy, *Real Algebraic Geometry*, Ergebrisse der Mathematik und ihser Grenzgebiete, Springer, Berlin, 1998.

[50] Y. Yu, J. Peng and S. Yue, "A new nonconvex approach to low-rank matrix completion with application to image inpainting," *Multidim. Syst. Sign. Process.*, vol. 30, pp. 145-174, 2019.

[51] I. Ram, M. Elad and I. Cohen, "Image processing using smooth ordering of its patches," *IEEE Trans. Image Process.*, vol. 22, no. 7, pp. 2764-2774, 2013.

[52] Z. Zhang and H. He, A customized low-rank prior model for structured cartoon-texture image decomposition," *Signal Processing: Image Communication*, vol. 96, 116308, 2021.

[53] H.-Y. Yan, Y.-M. Huang and Y. Yu, "A matrix rank minimization-based regularization method for image restoration," *Digit. Signal Process.*, vol. 130, 103694, 2022.

[54] Z. Wang, A. C. Bovik, H. R. Sheikh and E. P. Simoncelli, "Image quality assessment: from error visibility to structural similarity," *IEEE Trans. Image Process.*, vol. 13, no. 4, pp. 600-612, 2004.